Electronic transport in ferroelectric-ferromagnetic composites $La_{5/8}(Ba,Ca)_{3/8}MnO_3:LuMnO_3$

P. Mandal,[1] P. Choudhury,[2] and B. Ghosh[1]
[1]*Saha Institute of Nuclear Physics, 1/AF Bidhannagar, Calcutta 700 064, India*
[2]*Central Glass and Ceramic Research Institute, 196 Raja S. C. Mullick Road, Calcutta 700 032, India*
(Received 5 July 2005; revised manuscript received 29 May 2006; published 19 September 2006)

An almost complete immiscibility between metallic ferromagnet $La_{5/8}Ba_{3/8}MnO_3$ or $La_{5/8}Ca_{3/8}MnO_3$ and insulating ferroelectric $LuMnO_3$ has been established from structural, magnetic, and transport studies. Both $(x)La_{5/8}Ba_{3/8}MnO_3:(1-x)LuMnO_3$ and $(x)La_{5/8}Ca_{3/8}MnO_3:(1-x)LuMnO_3$ show a metal-insulator transition below a critical volume fraction x_{vc} of the metallic component. Over the entire range of $x>x_{vc}$, electronic conduction follows a classical percolation model. The conductivity scaling exponent t is the same as that of the universal value (=2) for the three-dimensional (3D) system; x_{vc} is also close to the theoretical prediction for the 3D continuum model. For $x<x_{vc}$, the transport phenomenon is dominated by the insulating $LuMnO_3$. The temperature dependence of both resistivity and thermopower for $0\leq x<x_{vc}$ shows that the conduction is due to the thermal activation of charge carriers with a band gap ~0.5 eV.

DOI: 10.1103/PhysRevB.74.094421 PACS number(s): 75.47.Lx, 72.60.+g, 75.50.Cc

I. INTRODUCTION

The possibilities of chemical substitution in perovskite manganites $RMnO_3$ (R=rare-earth metals) with iso- and heterovalent ions have opened a wide area for systematic studies of their physical properties by continuous variation of the intrinsic parameters, such as ionic size, valence state, etc. Above a critical value of ionic radius r_R of R, the crystal structure of $RMnO_3$ is orthorhombic but hexagonal below this critical ionic size. As the physical properties are sensitive to structural parameters, one finds dramatic changes in different physical properties with the change of ionic radius. For example, orthorhombic $LaMnO_3$ with a maximum r_R shows A-type antiferromagnetic ordering and cooperative Jahn-Teller distortion while hexagonal $LuMnO_3$ (LMO) with minimum r_R shows a ferroelectric ordering below 900 K and a paramagnetic to complicated antiferromagnetic (AFM) phase transition at around 90 K.[1–9] Substitution of R^{3+} by M^{2+} (M=Sr,Ca,Ba,Pb) in orthorhombic $RMnO_3$ brings about remarkable changes in the physical properties; while $RMnO_3$ is an AFM Mott-Hubbard insulator, the $R_{1-x}M_xMnO_3$ materials are ferromagnetic (FM) metal above a critical doping (x). However, in many cases the substitution of R in $RMnO_3$ by divalent or other rare-earth elements is limited by the solubility factor. While exploring the possibility of doping Lu in $La_{5/8}Sr_{3/8}MnO_3$ (LSMO), Park *et al.*[10] observed chemical immiscibility between FM-metallic LSMO and FE-insulating LMO. Nonetheless, it resulted in a new kind of composite material in which the transport properties exhibit a percolation behavior.

In the present work, we explore the possibility of doping Lu in FM materials $La_{5/8}Ba_{3/8}MnO_3$ (LBMO) and $La_{5/8}Ca_{3/8}MnO_3$ (LCMO). Similar to LSMO:LMO, we have also observed chemical immiscibility in (x)LBMO:$(1-x)$LMO and (x)LCMO:$(1-x)$LMO from x-ray and magnetization analyses. The temperature dependence of resistivity and thermopower has been studied over a wide range of temperature for samples with different compositions (x). Above a critical volume fraction of the metallic component, the dependence of resistivity on x has been analyzed using a classical percolation model.

II. SAMPLE PREPARATION AND EXPERIMENTAL TECHNIQUES

We prepared polycrystalline samples of two series: $(x)La_{5/8}Ba_{3/8}MnO_3:(1-x)LuMnO_3$ and $(x)La_{5/8}Ca_{3/8}MnO_3:(1-x)LuMnO_3$. For each series, as many as 20 samples with different molar ratios were prepared by standard solid-state reaction method. The well-mixed powder of carbonates and oxides were heated at 1300–1350 °C in air for several days with intermediate grindings. Finally, the powder was pressed into pellets and heated at 1350–1400 °C for more than 48 h in oxygen atmosphere, followed by an additional overnight annealing at 550 °C in the same atmosphere to ensure oxygen content close to 3.

Samples were characterized by x-ray powder diffraction with Cu$K\alpha$ radiation. Magnetization at 5 K as a function of field up to 5 T was measured using a SQUID magnetometer (Quantum Design) while the magnetic transition was measured using an ac susceptometer. Resistivity measurements were performed with a standard dc four-probe method in the temperature range 20–425 K. The thermopower was measured by the differential dc technique from about 330 K down to liquid nitrogen. In this method, a small temperature difference between the two ends of the sample was produced by a resistive heater attached to one end of the sample, and was measured by a chromel-alumel thermocouple.

III. EXPERIMENTAL RESULTS AND DISCUSSION

A. X-ray diffraction

All samples were characterized by powder x-ray diffraction and no impurity phase was observed. The diffraction spectra were collected at room temperature in a step-scan mode with a step size 0.02° over a prolong period so that the relative intensity ratio can be determined accurately for the terminal compositions. We have performed Rietveld analysis to calculate the lattice parameters for $La_{5/8}Ba_{3/8}MnO_3$, $La_{5/8}Ca_{3/8}MnO_3$, and $LuMnO_3$. The peak positions of $La_{5/8}Ba_{3/8}MnO_3$ correspond to a rhombohedral unit cell with a=5.52 and c=13.5157 Å in hexagonal indexing while the

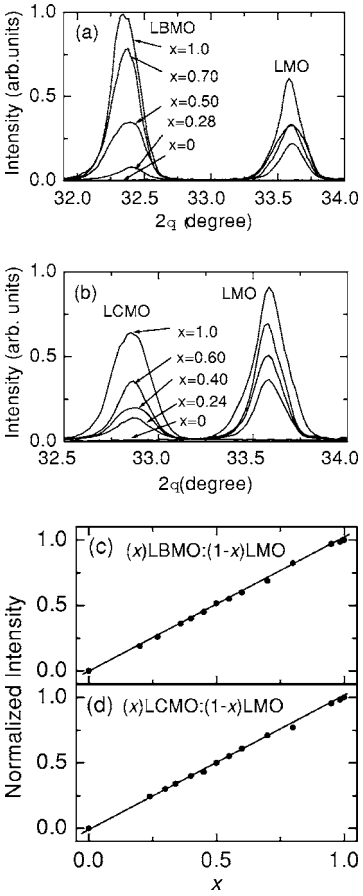

FIG. 1. Powder x-ray diffraction intensity vs 2θ for (a) (x)LBMO:$(1-x)$LMO and (b) (x)LCMO:$(1-x)$LMO. The peaks with maximum intensity, viz., (104) for LBMO, (112) for LCMO, and (211) for LMO, are shown. Normalized intensity (see text) vs metallic molar ratio x for (c) (x)LBMO:$(1-x)$LMO and (d) (x)LCMO:$(1-x)$LMO.

crystal symmetry of $La_{5/8}Ca_{3/8}MnO_3$ is orthorhombic with lattice parameters $a=5.4445$, $b=5.4591$, and $c=7.6923$ Å. $LuMnO_3$ shows hexagonal symmetry with space group $P6_3cm$. The calculated lattice parameters $a=6.0406$ and $c=11.3695$ Å are close to the earlier report.[2] Figures 1(a) and 1(b) show the variation of x-ray intensity for mixed specimens (x)LBMO:$(1-x)$LMO and (x)LCMO:$(1-x)$LMO, respectively. Mixed compositions (x)LBMO:$(1-x)$LMO show peaks due to rhombohedral and hexagonal phases of LBMO and LMO, respectively. Similarly, (x)LCMO:$(1-x)$LMO show those peaks observed only in the parent compounds LCMO and LMO. With decreasing x, the intensity of the peaks corresponding to LBMO (LCMO) phase decreases while that for LMO phase increases monotonically. Though the relative intensities of the peaks of different phases systematically change with x in both of the composites, the diffraction peak positions hardly shift with varying composition. That is, the lattice parameters of the individual phases do not change in mixed compositions.

From the variation of relative intensity with x, one can determine LBMO(LCMO):LMO composition ratio and compare it with nominal composition. For this quantitative phase analysis, first we have selected the peaks with maximum intensity for LBMO, LCMO, and LMO at around $2\theta=32.35$, 32.85, and 33.58°, respectively. The peak intensity of LMO in LCMO:LMO with $x=0.5$ composition has then been multiplied by a factor 0.59 to have equal intensity values for the strongest peaks of LCMO and LMO phases in this sample. The peak intensity of LMO for other compositions has also been multiplied by 0.59. Coincidentally, the peak intensity ratio for LBMO:LMO with $x=0.5$ has been found to be close to 1. After this scaling, the normalized intensity $I_n(x)=I_{LCMO}/(I_{LCMO}+I_{LMO})$ for different compositions is calculated. Similar calculation is also done for (x)LBMO:$(1-x)$LMO. I_n versus x for both the systems is almost linear and passes through the origin with a slope 1 [Figs. 1(c) and 1(d)]. So, the starting composition and the composition determined by x-ray analysis are close to each other. Even for $x=0.985$, we observe finite intensity at 33.58° for LMO and the normalized intensity is close to the expected value. Thus an almost complete immiscibility exists within a mixture of two compounds similar to that observed in (x)LSMO:$(1-x)$LMO in which polarized optical microscopy directly revealed the μm-scale phase separation.[10]

B. Magnetization

We have performed magnetic measurements to understand the nature of magnetic properties and to determine the magnetic transition temperature of LBMO:LMO and LCMO:LMO composites. As LBMO and LCMO are FM metal while LMO is an AFM insulator, one can estimate the volume fraction of FM phase from the saturation magnetization measurements. The field (H) dependence of magnetization (M) at 5 K is shown in Figs. 2(a) and 2(b). For both systems initially M increases sharply with magnetic field and then saturates at higher fields for all samples with $x>0$. The variation of saturation magnetization (M_S) (normalized with respect to the $x=1.0$ sample) with composition (x) is shown in Figs. 2(c) and 2(d). It is clear that M_S increases linearly with x for both the composites LBMO:LMO and LCMO:LMO. The variation of M_S with x is similar to that of x-ray intensity. Over the whole range of compositions, magnetization data fall on the straight line. Unlike previous reports on LSMO:LMO, we have not seen any deviation of magnetization data for samples with higher x.[10] It is speculated that the deviation in M_S for $0.5\leq x\leq 0.8$ is due to a small deviation from stoichiometric composition in LSMO. The immiscibility between FM and FE phases may also be tested by studying the variation of FM transition temperature T_C as a function of x. Figures 2(e) and 2(f) show the variation of T_C with composition for LBMO:LMO and LCMO:LMO specimens. T_C was determined from the low-field magnetization as well as from the transport measurements. T_C is defined as the temperature at which ρ increases and M decreases sharply with increasing T, i.e., $d\rho/dT$ and dM/dT show extrema. One can see from Fig. 2(f) that T_C determined from magnetization and transport measurements are close to each other. For LBMO:LMO composite, T_C was determined only from transport data. T_C for $La_{5/8}Ba_{3/8}MnO_3$ and $La_{5/8}Ca_{3/8}MnO_3$ are 341 and 261 K, respectively. It is clear that for both systems T_C decreases quite rapidly as x is

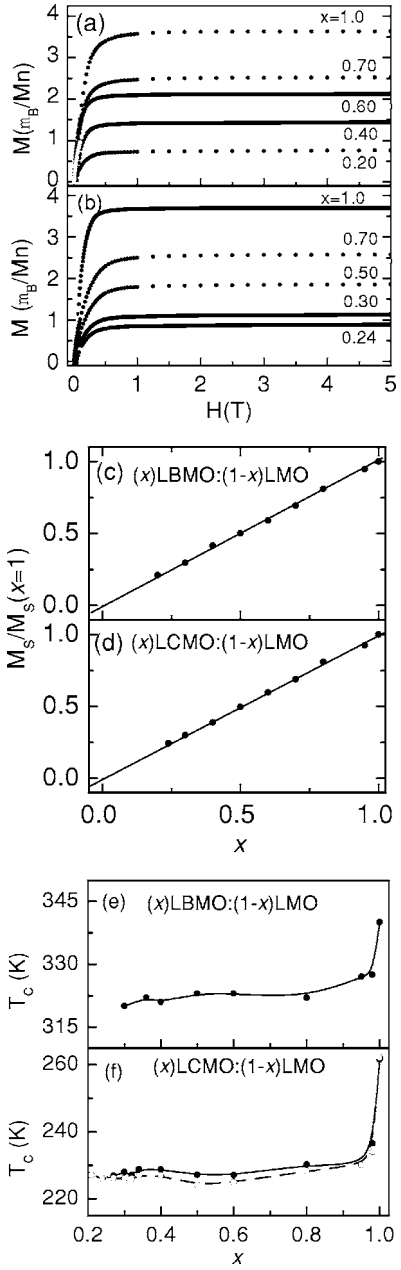

FIG. 2. Field dependence of magnetization at 5 K for (a) (x)LBMO:$(1-x)$LMO and (b) (x)LCMO:$(1-x)$LMO. Variation of saturation magnetization at 5 T with metallic molar ratio x for (c) (x)LBMO:$(1-x)$LMO and (d) (x)LCMO:$(1-x)$LMO. Composition dependence of ferromagnetic transition temperature (T_C) for (e) (x)LBMO:$(1-x)$LMO and (f) (x)LCMO:$(1-x)$LMO. For (x)LCMO:$(1-x)$LMO, T_C was determined from transport (closed symbol) and magnetic (open symbol) measurements. The lines are guide to the eye.

decreased from 1 to 0.985. However, after this rapid decrease, T_C remains fairly insensitive for all other compositions for both systems. Similar behavior has also been reported for LSMO:LMO composites.[10] From these results it is clear that solubility of LMO in LBMO, LCMO, and LSMO is less than 1.5%.

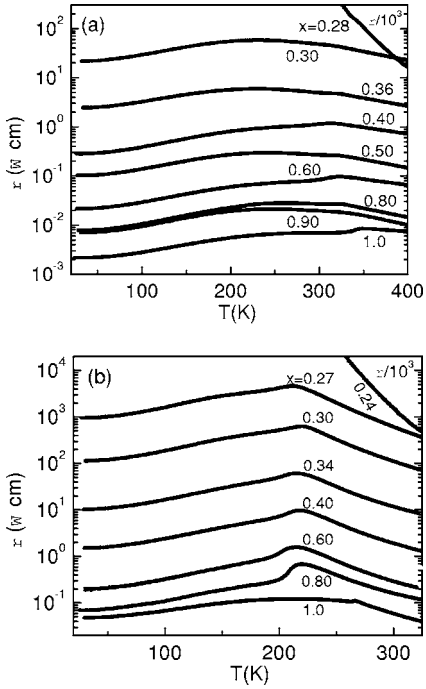

FIG. 3. Temperature dependence of resistivity for different metallic molar ratios x: (a) (x)LBMO:$(1-x)$LMO and (b) (x)LCMO:$(1-x)$LMO.

C. Resistivity and thermopower

In a binary mixture of metal and insulator, the conduction phenomenon can be described by percolation theory. In (x)LSMO:$(1-x)$LMO with micrometer-sized particles, it has been shown that the resistivity obeys classical percolation behavior. We have investigated the temperature and composition dependence of resistivity for both LBMO:LMO and LCMO:LMO series (Fig. 3). The temperature dependence of ρ for LBMO and LCMO ($x=1.0$) samples is as expected. However, in both series, ρ at a given T increases continuously with the increase of LMO content $(1-x)$ in the samples. The increase of ρ with the decrease of x is due to the increase of the length of conducting paths in the system to avoid the insulating grains. As the numbers of metallic grains decrease with the increase of LMO, the length of the conducting paths increases and the number of conducting paths between voltage terminals decreases. When LMO content reaches a critical value (x_c), ρ increases sharply by a few orders of magnitude and the T dependence of ρ changes from metalliclike to semiconductinglike. So a metal-insulator (MI) transition occurs at x_c. One expects that the T dependence of ρ for samples above x_c should be dominated by the FM component and that below x_c by LMO. The overall T dependence of ρ is more or less similar for samples in the metallic regime, although the absolute value of ρ changes by several orders of magnitude in both series. In LBMO:LMO, for x just below the critical value ~ 0.30 the nature of the $\rho(T)$ curve below T_C changes dramatically [Fig. 3(a)]. For $x=0.30$, $\rho(T)$ is metalliclike down to 15 K while for $x=0.28$, ρ increases very rapidly with decreasing temperature and its value is so high that we are unable to measure below 150 K.

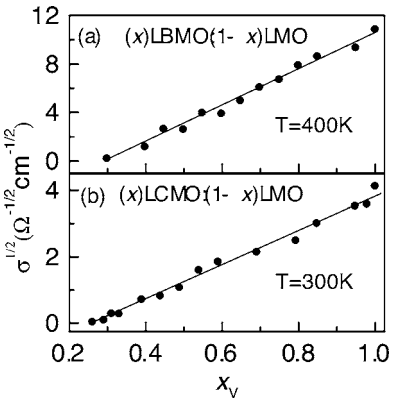

FIG. 4. Square-root of conductivity ($\sigma^{1/2}$) vs metallic volume fraction x_v: (a) (x)LBMO:$(1-x)$LMO and (b) (x)LCMO:$(1-x)$LMO. Solid lines represent linear behavior.

This suggests that the MI transition in the LBMO:LMO system occurs close to $x=0.30$. A qualitatively similar behavior is observed in the case of the LCMO:LMO system for x around 0.25 [Fig. 3(b)].

One can obtain a better understanding of the transport properties of insulator-conductor composites by analyzing the nature of the dependence of ρ on the concentration of metallic component x. According to the standard theory of transport in isotropic percolating materials, the bulk conductivity σ of a composite with volume concentration x_v of the conducting phase obeys a scaling law of the form[11,12]

$$\sigma = \sigma_0 (x_v - x_{vc})^t, \tag{1}$$

where σ_0 is a proportionality constant, x_{vc} is the percolation threshold volume of the metallic phase, and t is the transport critical exponent. The exponent t depends on the dimensionality of the system and its value is 2 for the three-dimensional network.[14–17] In LSMO:LMO, the electronic conduction follows nonuniversal percolation below T_C due to the intergrain tunneling conduction while it crosses over to universal behavior above T_C.[10] To understand the nature of percolation in LBMO:LMO and LCMO:LMO, the values of σ at 400 and 300 K, respectively (i.e., conductivities well above the ferromagnetic transition), are fitted using Eq. (1). x_v is calculated from the knowledge of the unit-cell densities of each parent compound. For both of the composites, the best fit reveals t close to the universal value 2; for LBMO:LMO, $t = 2.03$ and for LCMO:LMO it is 1.98, with an error less than 5% in both of the cases. This persuades a linear $\sigma^{1/2}$ versus x_v dependence [Figs. 4(a) and 4(b)]. Normally, Eq. (1) is valid in a small regime just above the percolation threshold in which the critical fluctuations extend over distances much larger compared to the characteristic size of the constituents. However, the validity of Eq. (1) well above the percolation threshold can be reconciled with the theory of 3D site percolation.[13]

Contrary to σ_0 and x_{vc}, which depend on microscopic details such as the microstructure and the mean intergrain junction conductance, the exponent t is expected to be material-independent.[11] The universality of t is indeed confirmed by various numerical calculations of random-resistor network models.[14–17] From the fit we find $x_{vc}=0.30$ and 0.26 for LBMO:LMO and LCMO:LMO, respectively (Fig. 4). This is consistent with the observed MI transition in Fig. 3. The values of percolation threshold of the metallic phase x_{vc} are within the range of theoretical predictions of three-dimensional continuum percolation models. According to these models, x_{vc} is 0.29 when the metallic volume is permitted to overlap, and 0.15 if overlapping is not allowed.[18] Thus for both of the composites the percolation threshold is close to the critical value for the overlap case. The slightly larger value of x_{vc} for LBMO:LMO than LCMO:LMO may be the implication of the effect of ionic size on percolation phenomenon. Due to the larger ionic size of Ba than Ca, LBMO has a larger molar volume as compared to LCMO in the composite. As the ionic size of Sr is larger than Ca but smaller than Ba, x_{vc} for LSMO:LMO is expected to lie in between 0.26 and 0.30. However, for the LSMO:LMO composite x_{vc} is observed to be 0.224.[10] One possible reason for this discrepancy may be the quality of samples for $x \geq 0.40$, which show a smaller value of saturation magnetization than expected. Normally, samples with smaller M_s are inferior in quality and have low conductivity. In such cases, fitting with Eq. (1) may result in a lower value of x_{vc}. There may be another possibility also. In LSMO:LMO, percolation parameters were determined using resistivity data at 400 K, which in the scale of reduced temperature (T/T_C) is 1.12.[10] Figure 4(a) in Ref. 10 clearly indicates that t is likely to decrease even above 400 K. We believe that by using resistivity data at temperatures well above T_C, one might obtain both t and x_{vc} closer to that of theoretical prediction. It may be noted that the percolation parameters for LBMO:LMO and LCMO:LMO composites are determined at reduced temperatures 1.24 and 1.32, respectively, which are higher than that for LSMO:LMO. To establish firmly the role of ionic size on x_{vc} for 3D site percolation, one needs a systematic study of the percolation phenomenon as a function of rare-earth site ionic size, say, by replacing La with other smaller elements such as Pr, Nd, etc.

Although our results are close to the theoretical predictions, confirmations to the standard percolation theory of transport universality are found only in a limited number of experiments on real disordered composites. Recently, Vionnet-Menot *et al.*[19] composed a huge number of experimental data on critical exponent t and threshold x_{vc} measured in various composites including carbon-black-polymer systems, oxide-based thick film resistors, and other metal-inorganic and metal-organic insulator composites. They observed a lack of universality in the critical exponent in many systems. For the vast majority of cases, the critical exponent is larger than 2 and there is no correlation between t and x_{vc}. This nonuniversality of t is not limited to a particular class of materials. However, the granular metals have somewhat less spread values of t around 2 as compared to other composites. In this respect, the present system is close to the granular metals.

As stated earlier, the validity of the scaling law holds well over a wide range of composition beyond the percolation threshold. This demands consideration of a generalized effective-medium theory. To analyze the transport coefficient of a binary mixture, Mclachlan[20] proposed an effective-

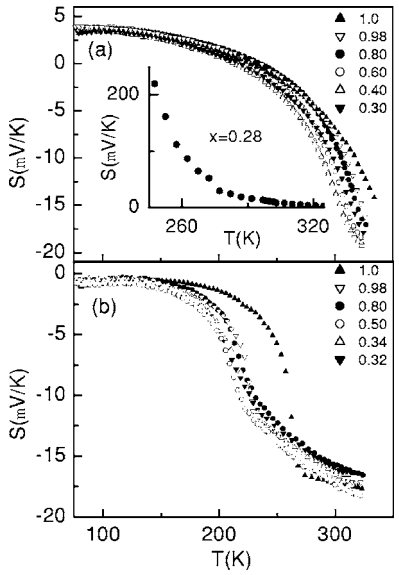

FIG. 5. Temperature dependence of thermopower (S) for different metallic molar ratios x: (a) (x)LBMO:$(1-x)$LMO and (b) (x)LCMO:$(1-x)$LMO. Inset shows T dependence of S for (x)LBMO:$(1-x)$LMO close to percolation threshold (S is large and remains positive at high temperatures).

medium approach in which the effective conductivity of the mixture is given by

$$(1-x_v)\left(\frac{\sigma_I^{1/t}-\sigma_E^{1/t}}{\sigma_I^{1/t}+A\sigma_E^{1/t}}\right)+x_v\left(\frac{\sigma_M^{1/t}-\sigma_E^{1/t}}{\sigma_M^{1/t}+A\sigma_E^{1/t}}\right)=0, \qquad (2)$$

where σ_M and σ_I are the conductivities of the components M and I, respectively, and $A=(1-x_{vc})/x_{vc}$. This equation has been successfully applied to isotropic inhomogeneous media in a wide x_v region including the percolation regime.[20–22] In manganites too, effective-medium theory has been applied to explain temperature and composition dependence of electrical and thermal transport coefficients such as resistivity, thermopower, thermal conductivity (κ), etc.[23–25] both above and below the MI transition. Irrespective of the origin and the nature of the insulating phase, the effective-medium theory holds well to explain the transport properties in manganites. In the present case, the resisitivity of $LuMnO_3$ is so high that we may effectively consider $\sigma_I=0$. So Eq. (2) reduces to $\sigma_E=\sigma_M(x_v-x_{vc})^t/(1-x_{vc})^t$, which is the well-known power-law form of the bulk conductivity in isotropic percolating materials. Considering $t=2$ (three-dimensional network), a $\sigma_E^{1/2}$ versus x_v plot would give a straight line with a slope $\sigma_0^{1/2}=\sigma_M^{1/2}/(1-x_{vc})$. The conductivity data for LBMO:LMO and LCMO:LMO [Figs. 4(a) and 4(b)] clearly corroborate this slope identifying $t=2$ in these systems.

To gain further insights into the transport phenomena of this ferromagnetic and ferroelectric mixture, we have investigated the temperature dependence of thermopower of these samples (Fig. 5). Figures 5(a) and 5(b) show that for both systems, S is almost independent of composition for $x>x_{vc}$ except close to the vicinity of T_C, where S decreases rapidly with increasing temperature. The difference in S close to T_C is due to the small difference in transition temperatures, which is not systematic with x as we have already seen from other measurements. Below $x=x_{vc}$, both the magnitude and T dependence of S change drastically [inset to Fig. 5(a)]. S is large and positive and it decreases with increasing temperature both above and below T_C, i.e., semiconductinglike behavior.

When thermal and electronic transport properties of our systems are viewed as those of MI mixtures, it is important to investigate whether the temperature dependence of measured thermopower is consistent with the theoretical prediction of effective thermoelectric power S_E.[26] For an isotropic binary mixture, the effective thermopower S_E, in terms of σ, κ, and S of each component, is given by

$$S_E=S_M+(S_I-S_M)\left(\frac{\kappa_E/\kappa_M}{\sigma_E/\sigma_M}-1\right)\Bigg/\left(\frac{\kappa_I/\kappa_M}{\sigma_I/\sigma_M}-1\right), \qquad (3)$$

where κ_E and σ_E refer to effective thermal and electric conductivity, respectively, of the binary mixture. This equation has been successfully applied to explain the behavior of S in binary films.[21] In $La_{5/8-x}Pr_xCa_{3/8}MnO_3$ it has been shown that above x_{vc}, $\sigma_I/\sigma_M \ll \kappa_I/\kappa_M$.[23] Assuming a similar inequality holds for the present system, the above equation leads to $S_E=S_M$, which explains the experimental results in the metallic regime. On the other hand, S becomes equal to S_I when $\sigma_E=\sigma_I$ and $\kappa_E=\kappa_I$. This explains the large and semiconductinglike T dependence of S just below x_{vc}. The fact that S does not decrease with x above the percolation threshold (Fig. 5) may be understood as follows. As S is the ratio of thermo-emf and temperature difference, it does not depend on the geometry of the conducting paths connecting the volt-

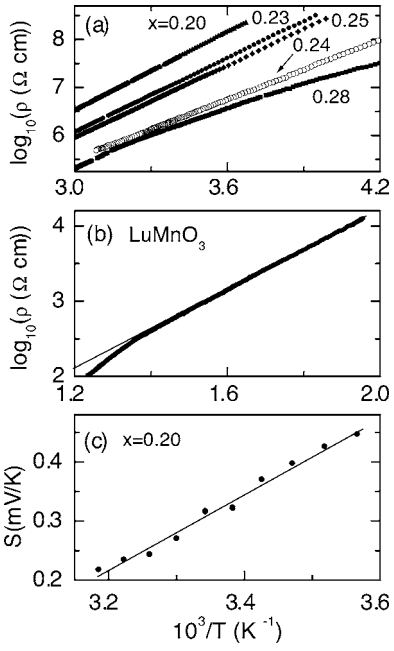

FIG. 6. (a) Temperature dependence of resistivity below x_{vc} for (x)LBMO:$(1-x)$LMO$(x=0.20,0.23,0.25,0.28)$ and (x)LCMO:$(1-x)$LMO $(x=0.24)$ samples. (b) Temperature dependence of resistivity for $LuMnO_3$. (c) Temperature dependence of thermopower for (x)LBMO:$(1-x)$LMO with $x=0.20$. Solid lines represent linear behavior.

age terminals, i.e., S is independent of both length and cross section of the conducting paths. In a binary mixture of metal and insulator, S is, therefore, independent of x and would show metalliclike temperature dependence as long as there are finite numbers of conducting paths between the voltage terminals but show T dependence of the insulator when no connecting paths exist.

It is evident from Figs. 3(a) and 3(b) that the behavior of the T dependence of ρ changes from metalliclike to semiconductinglike as x decreases from just above to just below x_c. As there is no conducting path through LBMO or LCMO grains connecting the voltage terminals, resistivity increases sharply below x_c. In such a situation, current has to pass through both metallic as well as insulating grains of LMO, i.e., current passes through a series network of metallic and insulating particles. Since the resistivity of LMO is too high compared to LBMO and LCMO, the effective resistivity of such a network is dominated by LMO. The linear behavior of $\log_{10}\rho$ versus $1/T$ and S versus $1/T$ with activation energy $E_0=0.55$ eV for both LBMO:LMO and LCMO:LMO composites below x_c supports this view (Fig. 6).

In summary, we have established almost complete immiscibility of ferroelectric $LuMnO_3$ in ferromagnetic LBMO and LCMO from x-ray, magnetization, resistivity, and thermopower studies. Both LBMO:LMO and LCMO:LMO composites exhibit a MI transition below a critical value of metallic volume fraction. The composition dependence of conductivity is explained within the framework of a 3D continuum percolation model with a critical exponent close to the universal value 2 as observed in most of the granular metals. In the metallic regime, the validity of the scaling law far beyond the critical region is explained by an effective-medium picture as in several other manganites. Below the percolation threshold, the temperature dependence of resistivity and thermopower is dominated by the thermal activation of carriers of $LuMnO_3$.

ACKNOWLEDGMENT

We thank A. Pal and D. Vieweg for technical support.

[1] See, for example, M. Imada, A. Fujimori, and Y. Tokura, Rev. Mod. Phys. **70**, 1039 (1998); J. M. D. Coey, M. Viret, and S. von Molnar, Adv. Phys. **48**, 167 (1999).
[2] T. Katsufuji, S. Mori, M. Masaki, Y. Moritomo, N. Yamamoto, and H. Takagi, Phys. Rev. B **64**, 104419 (2001).
[3] I. G. Ismailzade and S. A. Kizhaev, Fiz. Tverd. Tela (Leningrad) **7**, 298 (1965) [Sov. Phys. Solid State **7**, 236 (1965)].
[4] K. Lukaszewicz and J. Karut-Kalicinska, Ferroelectrics **7**, 81 (1974).
[5] N. A. Hill, Annu. Rev. Mater. Res. **32**, 1 (2002).
[6] F. A. Smolenski and I. E. Chupis, Sov. Phys. Usp. **25**, 475 (1982).
[7] J. Wang, J. B. Neaton, H. Zheng, V. Nagarajan, S. B. Ogale, B. Liu, D. Viehland, V. Vaithyanathan, D. G. Schlom, U. V. Waghmare, N. A. Spaldin, K. M. Rabe, M. Wuttig, and R. Ramesh, Science **299**, 1719 (2003).
[8] J. van Suchtelen, Philips Res. Rep. **27**, 28 (1972).
[9] H. Kitahata, K. Tadanaga, T. Minami, N. Fujimura, and T. Ito, Appl. Phys. Lett. **75**, 719 (1999), and references therein.
[10] S. Park, N. Hur, S. Guha, and S.-W. Cheong, Phys. Rev. Lett. **92**, 167206 (2004).
[11] D. Stauffer and A. Aharony, *Introduction to Percolation Theory* (Taylor and Francis, London, 1994).
[12] B. I. Shklovskii and A. L. Efros, *Electronic Properties of Doped Semiconductors* (Springer, New York, 1984).
[13] D. Adler, L. P. Flora, and S. D. Senturia, Solid State Commun. **12**, 9 (1973).
[14] G. G. Batrouni, A. Hansen, and B. Larson, Phys. Rev. E **53**, 2292 (1996).
[15] J.-M. Normand and H. J. Hermann, Int. J. Mod. Phys. C **6**, 813 (1995).
[16] J. P. Clere, V. A. Podolsky, and A. K. Sarychev, Eur. Phys. J. B **15**, 507 (2000).
[17] M. Sahimi, *Application of Percolation Theory* (Taylor and Francis, London, 1994).
[18] S. Kirkpatrick, Rev. Mod. Phys. **45**, 574 (1973).
[19] S. Vionnet-Menot, C. Grimaldi, T. Maeder, S. Strässler, and P. Ryser, Phys. Rev. B **71**, 064201 (2005), and references therein.
[20] D. S. McLachlan, J. Phys. C **20**, 865 (1987).
[21] G. Hurvits, R. Rosenbaum, and D. S. McLachlan, J. Appl. Phys. **73**, 7441 (1993).
[22] N. Dupez, D. S. McLachlan, and I. Sigalas, Solid State Commun. **66**, 869 (1988).
[23] K. H. Kim, M. Uehara, C. Hess, P. A. Sharma, and S.-W. Cheong, Phys. Rev. Lett. **84**, 2961 (2000).
[24] M. Jaime, P. Lin, S. H. Chun, M. B. Salamon, P. Dorsey, and M. Rubinstein, Phys. Rev. B **60**, 1028 (1999).
[25] G. H. Rao, J. R. Sun, Y. Z. Sun, Y. L. Zhang, and J. K. Liang, J. Phys.: Condens. Matter **8**, 5393 (1996).
[26] D. J. Bergman and O. Levy, J. Appl. Phys. **70**, 6821 (1991).